RSC Advances

ROYAL SOCIETY OF CHEMISTRY

www.rsc.org/advances

Journal Name

ARTICLE

Selectively hydrogenolysis of glycerol to 1,3-propanediol over egg-shell type Ir-ReO_x catalysts

Received 00th January 20xx,
Accepted 00th January 20xx

DOI: 10.1039/x0xx00000x

www.rsc.org/

Wenting Luo ,[a, c] Yuan Lyu,*[a] Leifeng Gong,[a] Hong Du,[a,c] Tao, Wang,[a,c] Yunjie Ding*[a,b]

The selective liquid-phase hydrogenolysis of glycerol to 1,3-propanediol is reported over egg-shell catalysts in which the loadings of Ir and Re were both 2 wt.%. The shell thickness can be tuned by impregnating a hydrophobic silanized support with an aqueous solution of precursors containing various concentrations of ethanol, using entrapped air to prevent the impregnation solution from entering into the support pellets. The conversion of glycerol for the target reaction over egg-shell catalysts was higher than that over a uniform catalyst, accompanied by a high selectivity for 1,3-propanediol over 1,2-propanediol. Reacting over the catalyst for which the ethanol concentration of the impregnation solution was 20 vol.% resulted in the best glycerol conversion (60.9%) and the highest yield of removal secondary hydroxyl group (30.2%). The properties of the egg-shell and uniform catalysts were characterized by XRD, TEM, XPS, H_2-TPR, H_2-pulse chemisorption and NH_3-TPD. An appropriate diffusion distance of reactants for egg-shell catalysts might result in better catalytic performance because of the high viscosity of the glycerol aqueous solution.

Introduction

As a sustainable biomass-derived product, glycerol has few environmental impacts compared with the energy- and emissions-intensive synthesis of fossil fuel-derived chemicals.[1-3] Glycerol is a byproduct of biodiesel produced from vegetable oils and animal fat,[4] and a large surplus glycerol has resulted from the rapid expansion of the global biodiesel production capacity.[5, 6] From an economic standpoint, the price decline of crude glycerol due to increasing biodiesel production makes glycerol an attractive material for the synthesis of fine chemicals.[7] Many processes have been developed to transform glycerol into different chemicals, such as oxidation, reforming, etherification, dehydration and hydrogenolysis.[8] Among these processing approaches, glycerol hydrogenolysis is one of the promising. The main products of glycerol hydrogenolysis are 1,3-propanediol, 1,2-propanediol, 1-propanol, and 2-propanol, and 1,3-propanediol has great economic value as the monomer of polytrimethylene terephthalate (PTT). Therefore, hydrogenolysis of glycerol to 1,3-propanediol has attracted more attention in recent years.[8]

Recently, Re has been added to different noble metal catalysts to improve their catalytic activity. Pt-Re, Rh-Re, Pd-Re, Ru-Re, and Ir-Re have all been investigated.[9-13] Among these catalyst systems, iridium modified with rhenium has demonstrated the best catalytic activity in glycerol hydrogenolysis. Tomishige et al. observed high selectivity for 1,3-propanediol on Ir-ReO_x/SiO_2 with an Ir loading of 4wt.% when reacted with the addition of a solid acid co-catalyst in a batch reactor.[14, 15] They proposed the following mechanism for Ir-ReO_x/SiO_2-catalyzed glycerol hydrogenolysis: Re-OH interacts with the OH groups of glycerol to form 2,3-dihydroxypropaneoxide; then, hydrogen species activate the secondary carbon of 2,3-dihydroxypropaneoxide to cleave the C-O bond; and hydrolysis occurs to release the product.[11, 14, 16, 17]

Egg-shell catalysts are pelletized catalysts in which the active phase is located on the outer surface. Egg-shell catalysts are broadly applied in many reactions, such as selective hydrogenation reactions[18-21], Fischer-Tropsch synthesis[22, 23], methane partial oxidation[24] and hydrodesulfurization[25]. To maintain an acceptable pressure gradient, pelletized catalysts of a certain size are usually required for reactions in industrial fixed-bed reactors, but uniform catalysts will sometimes limit the mass and/or heat transfer, which negatively affect catalytic performance. Egg-shell catalysts solve problems of gum formation, the generation of overheating spots in the reactor bed and the undesired complete reaction of reactants.[18-26]

To the best of our knowledge, few studies have investigated Ir egg-shell catalysts for glycerol hydrogenolysis. Glycerol is strongly adhesive, and internal diffusion probably affects the catalytic performance in glycerol hydrogenolysis. In this study, egg-shell catalysts were prepared by impregnating a hydrophobic silanized support with an aqueous solution of precursors containing various concentrations of ethanol, using entrapped air to prevent the impregnation solution from entering the support pellets. The properties of these egg-shell catalysts and uniform catalyst were investigated by several characterization techniques, including

[a] Dalian National Laboratory for Clean Energy, Dalian Institute of Chemical Physics, Chinese Academy of Sciences, 457 Zhongshan Road, Dalian, Liaoning, China. E-mail: dyj@dicp.ac.cn. Tel: +86 411 84379143; Fax: +86 411 84379143.
[b] State Key Laboratory of Catalysis, Dalian Institute of Chemical Physics, Chinese Academy of Sciences, 457 Zhongshan Road, Dalian, Liaoning, China.
[c] University of Chinese Academy of Sciences, No.19A Yuquan Road, Beijing 100049, China.

optical microscopy, X-ray powder diffraction (XRD), transmission electron microscopy (TEM), X-ray photoelectron spectroscopy (XPS), H_2-TPR (temperature-programmed reduction), H_2-pulse chemisorption and temperature-programmed desorption of ammonia (NH_3-TPD), and the catalytic performance of the egg-shell catalysts and uniform catalyst were all evaluated in glycerol hydrogenolysis.

Experimental

Catalyst preparation

The egg-shell catalysts were prepared by the method devised by Ding[22]. TMCS-SiO_2 was prepared by silanizing a SiO_2 support (8-10 mesh) with trimethylchlorosilane (TMCS). First, we mixed 100 ml of toluene and 2.5 g of TMCS and stirred them uniformly. Then, 5 g of SiO_2 was adding to this mixture, which was refluxed for 16 h. We filtered the above material and washed it with ethanol and cyclohexane. Finally, the material was dried at 393 K for 8 h in air to obtain TMCS-SiO_2.

TMCS-SiO_2 was impregnated in a mixture of an aqueous solution of H_2IrCl_6 and ethanol, in which the ethanol concentration was 20, 25 or 30 vol.%. These treated samples were heated in a rotary evaporator at 313 K for 2 h, followed by drying at 393 K for 8 h in an oven and calcination at 773 K for 3 h. Then, Re was deposited on these materials with an aqueous solution of NH_4ReO_4. The above material was dried at 393 K for 12 h and calcinated at 773 K for 3 h, and the egg-shell catalysts were obtained using the impregnation solution with different concentrations of ethanol, which were denoted as RI20, RI25 and RI30, respectively. For comparison, a uniform catalyst was prepared by impregnating an aqueous solution of H_2IrCl_6 and NH_4ReO_4 in sequence with silica gel without any treatments. This uniform catalyst was denoted RI. RI was broken up and put through a series of graded sieves, and the resulting fractions were denoted as RI-sm-n (m and n correspond to the lower and upper mesh numbers of pellet size, respectively). RI20-s60-80 was prepared by the same method as RI20 with silica supports of 60-80 mesh. The contents of iridium and rhenium in all catalysts were 2 wt.%.

Catalytic performance test

Glycerol hydrogenolysis reactions were performed in a trickle bed reactor (9 mm i.d.) using 1.5 g of catalyst. The hydrogen flow was 40 ml·min^{-1}, which corresponded to a space velocity of 1600 ml·(h·g)$^{-1}$, and the glycerol flow was 0.65 ml·h^{-1}, which corresponded to a space velocity of 0.44 ml·(h·g)$^{-1}$. Before reaction, all catalysts were reduced at 463 K. The reactions were conducted at 403 K and 8 MPa. The gaseous products from the effluent were analyzed on-line using an Agilent GC-7890. The liquid-phase products were quantified by an internal standard method, and the internal standard substance was n-butyl alcohol. Then, the liquid-phase products were esterified by acetic anhydride catalyzed by pyridine and heated to 328 K for 1.5 h. The samples were quantified on a gas chromatograph (Agilent 7890) fitted with a flame ionization detector and a HP-5 capillary column.

The conversion of glycerol and the selectivity of the products were calculated by the following equations:

Conversion of glycerol (%) =

$$\frac{\text{moles of glycerol initially added} - \text{moles of glycerol that remained}}{\text{moles of glycerol initially added}} \times 100$$

Selectivity (%) =

$$\frac{\text{C mole of specific product}}{\text{sum of C mole of glycerol consumed}} \times 100$$

The removal selectivity of primary (or secondary) hydroxyl group (%) ($S_{1\text{-}OH}$ or $S_{2\text{-}OH}$) =

$$\frac{\text{sum of removal primary or secondary hydroxyl group}}{\text{sum of removal hydroxyl group}} \times 100$$

The yield of removal secondary hydroxyl group (%) ($Y_{2\text{-}OH}$) =

Conversion of glycerol × removal selectivity of secondary hydroxyl group

Characterizations

XRD data were collected on an X'pert PRO/PANalytical diffractometer with CuK_α radiation. The X-ray patterns were measured over a 2θ range of 10°-80° at 40 kV and 40 mA.

The particle size of the samples was observed by TEM using a JEM-2100 microscope operated at an accelerating voltage of 200 kV. The catalysts were ground and placed on a copper grid after being briefly dispersed in ethanol with ultrasonication.

XPS data were collected on a Thermo ESCALAB 250Xi equipped with a monochromatized AlK_α radiation (1486.6 eV, 15 kV, 10.8 mA). The pressure in the analysis chamber was approximately 7.1×10^{-5} Pa.

TPR analyses were performed on an AMI-300 catalyst characterization system. Approximately 100 mg of each sample was placed into quartz reactors and reduced under a stream of H_2 at 30 ml·min^{-1} (10 vol.% in Ar) from 323 to 773 K at a heating rate of 10 K·min^{-1}.

Optical micrographs were observed by optical microscopy, and the images were captured by a camera. The sample was the cross-sections of catalyst pellets prepared by cutting. The magnification of the objective and eyepiece were both 4. The image ruler was determined using the diameter of the catalyst pellets as a reference. The diameters of the catalyst pellets were measured by a Vernier calliper.

H_2-chemisorption was performed on an AMI-300 catalyst characterization system. Approximately 100 mg of the catalyst samples were reduced under a flow of 10% H_2/Ar at 463 K for 2 h, followed by purging with argon at 463 K for 0.5 h. Then, the samples were cooled to 313 K to be used for pulse adsorption. The adsorbed gas was 10% H_2/Ar, and the carrier gas was argon.

NH_3-TPD was carried out on an AMI-300 catalyst characterization system equipped with a thermal conductivity detector (TCD). A 100 mg sample was pre-treated in an Ar flow at 873 K for 0.5 h. Then, after cooling to 373 K under a continuous flow of argon, ammonia adsorption was performed by introducing a flow of 5% NH_3/Ar for 2 h using the static adsorption method. To remove all the physically adsorbed ammonia, the sample was purged with a helium flow of

Table 1 Catalytic performance of the glycerol hydrogenolysis over the RI, RI20, RI25 and RI30 catalysts[a]

catalyst	Conv. /%	selectivity/%						Carbon balance/%	1,3-PD/1,2-PD[g]	$Y_{2\text{-}OH}$/%[h]
		1,3-PD[b]	1,2-PD[c]	1-PO[d]	2-PO[e]	C_3H_8	Others[f]			
RI	48.9	37.0	12.9	35.6	9.0	4.9	0.6	100.9	2.9	24.6
RI20	60.9	31.1	7.5	45.4	9.1	6.6	0.3	94.7	4.1	30.2
RI25	56.6	31.9	8.6	42.9	9.3	6.8	0.5	101.4	3.7	27.9
RI30	53.7	32.1	9.3	33.5	8.1	16.7	0.3	95.0	3.5	25.3

[a] Reaction condition: P=8.0 MPa, T= 403 K, WHSV= 0.5 h^{-1}, 1.5 g catalyst, 80 wt% glycerol aqueous solution, V_{H2} = 40 ml/min, TOS= 36 h. [b] 1,3-PD = 1,3-propandiol, [c] 1,2-PD = 1,2-propanediol, [d] 1-PO = 1-propanol, [e] 2-PO = 2-propanol. [f] Others include ethanol, ethane and methane. [g] The ratio of selectivity of 1,3-propanediol to 1,2-propanediol, [h] The yield of removal secondary hydroxyl group. Reduction condition: P=1 atm, V_{H_2}= 40ml/min, T=463 K, TOS=2h.

30 ml·min^{-1} at 373 K for 0.5 h. Then, the NH_3-TPD pattern was recorded by heating from 373 to 873 K with a ramp of 10 K/min in an Ar flow, and the desorbed NH_3 was simultaneously monitored by online TCD analysis.

Results and discussion

Catalytic activity measurements

The activity of glycerol hydrogenolysis over the RI, RI20, RI25 and RI30 catalysts is summarized in Table 1. Approximately 60.9% glycerol conversion with 31.1% selectivity for 1,3-propanediol was obtained over the RI20 catalyst, which was impregnated in an aqueous solution of H_2IrCl_6 with a 20 vol.% ethanol concentration, followed by an aqueous solution of NH_4ReO_4 at 403 K with 8.0 MPa of H_2 pressure in an aqueous solution of 80% glycerol. Compared with the uniform catalyst (RI), the glycerol conversion of the RI20 catalyst increased from 48.9 to 60.9%, and the selectivity of 1,3-propanediol decreased from 37.0 to 31.1%. All the egg-shell catalysts (RI20, RI25 and RI30) showed better glycerol conversion than RI, accompanied with slightly lower selectivity for 1,3-propanediol. For the three egg-shell catalysts, the glycerol conversion increased from 53.7 to 60.9% with the decrease in the ethanol concentration from 30 to 20 vol.%.

Table 2 Catalytic performance of the hydrogenolysis of 1,3-propanediol over the RI and RI20 catalysts[a]

catalyst	Conv. /%	selectivity/%		
		1-PO	C_3H_8	Others
RI	40.6	91.0	8.5	0.5
RI20	43.0	95.8	3.7	0.5

[a] Reaction condition: P=8.0 MPa, T= 403 K, WHSV= 0.533 h^{-1}, 1.5 g catalyst, 80 wt% 1,3-propanediol aqueous solution, V_{H2} = 40 ml/min, t= 36 h. Reduction condition: P=1 atm, V_{H_2}= 40 ml/min, T=463 K, t=2 h.

In addition, 1,3-propanediol and 1,2-propanediol are the products of the parallel reaction of the first step of glycerol hydrogenolysis. Lower temperature would thermodynamically favour the selectivity for 1,3-propanediol over 1,2-propaendiol.[27] The short diffusion distance would also lead to better heat diffusion from the catalyst surface. Therefore, overheating on the catalytic active sites would be prevented, and the generation of undesired by-products (1,2-propanediol) would also be restricted. This is consistent with the reaction results. The 1,3-propanediol/1,2-propanediol ratios of RI20 and RI were 4.1 and 2.9, respectively, and the other egg-shell catalysts also produced a larger 1,3-propanediol/1,2-propanediol ratio than that of the uniform catalyst RI. Table 2 shows the results of the hydrogenolysis of 1,3-propanediol over the RI and RI20 catalysts. The conversion of 1,3-propanediol over the RI20 catalyst was higher than over the RI catalyst primarily because this reaction is consecutive and the active sites of glycerol hydrogenolysis and 1,3-propanediol hydrogenolysis both lie at the interface of the iridium and rhenium species.[14, 28, 29] Therefore, the yields of removal secondary hydroxyl groups ($Y_{2\text{-}OH}$) given in Table 1 can express the ability to remove secondary hydroxyl groups. This removal yield for the RI20 catalyst was 30.2%, much larger than that of the RI catalyst (24.6%). Therefore, the removal ability of 2-OH for the RI20 sample was better than the RI catalyst, which was mainly due to the high conversion of the RI20 catalyst. To determine how egg-shell catalysts produce high glycerol conversion, we conducted the following catalyst characterizations and experiments.

Catalysts characterizations

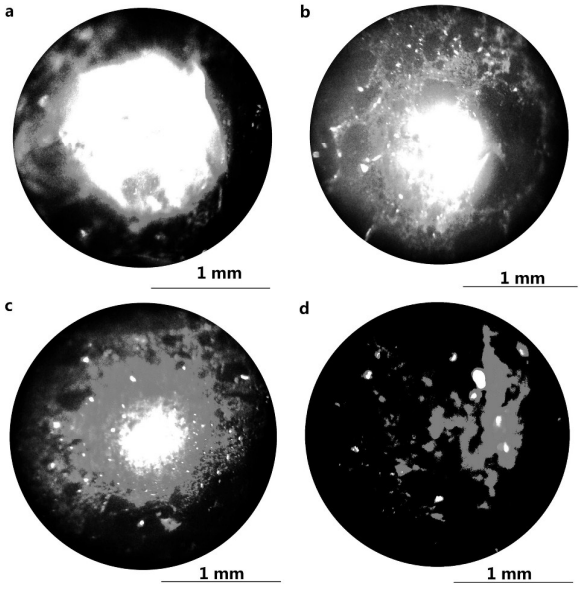

Figure 1 Optical micrographs of cross sections of catalysts. (a) RI20, (b) RI25, (c) RI30 and (d) RI.

Optical micrographs of catalyst cross-sections are shown in Figure 1. Black part of the circle section was where Ir species loaded on, and the white center was the part without supported Ir species. The active component of the uniform catalyst spread to every part of the pellet. The RI20 catalyst had the thinnest active component layer of approximately 0.4 mm. The thickness of shell for the RI25 and RI30 catalysts were approximately 0.7 and 1.0 mm. Combined with the results in Table 1, when a higher concentration of ethanol was used to prepare the catalysts, a thicker layer resulted, and the catalyst conversion was lower. The mass fraction of glycerol in the aqueous solution used in the reaction was 80%, which was highly viscous (85.00 Pa·s, 300K). Therefore, this hydrogenolysis reaction might be influenced by internal diffusion. To verify the influence of internal diffusion, the catalytic activities of the RI catalysts of different sizes were tested, and the results are shown in Table 3. The conversion of glycerol increased as the mesh of the catalysts decreased, and the conversion remained almost unchanged when the mesh of the catalysts decreased below 60. Egg-shell catalysts concentrate the active Ir component on their outer surface, which weakens the effect of internal diffusion. The conversion was higher when the shell was thinner, which might be due to difficult diffusion into the centre of the catalyst pellets. Glycerol may also react with hydrogen mostly on the outer surface of the catalyst pellets.

Table 3 Catalytic performance of the glycerol hydrogenolysis over the RI and RI20 catalysts in smaller mesh[a]

catalyst	Conv. /%	selectivity/%			
		1,3-PD	1,2-PD	1-PO	2-PO
RI-s10-20	52.7	34.2	9.8	41.9	10.9
RI-s20-40	54.5	33.5	9.5	42.2	11.0
RI-s40-60	57.4	31.5	8.7	41.8	9.1
RI-s60-80	56.4	32.9	9.7	37.6	10.7
RI20-s60-80	58.3	32	9.8	43.6	11.2
RI0.75-s20-40[b]	51.4	35.5	16.4	34.2	11.3

[a] Reaction condition: P=8.0 MPa, T= 403 K, WHSV= 0.5 h^{-1}, 1.5 g catalyst, 80 wt% glycerol aqueous solution, V_{H2} = 40 ml/min, t= 36 h. Reduction condition: P=1 atm, V_{H_2}= 40ml/min, T=463 K, t=2h. [b] Ir%=2wt%, Re%=1.5wt%, 20-40 mesh.

Although Ir was mainly distributed in the shell layer of the egg-shell catalysts, the silyl groups on the supports were wiped out after calcination at 773 K. Therefore, ReO_x was impregnated in the catalyst pellets using a common impregnation method without the existence of silyl groups. In other words, ReO_x should be distributed uniformly. Therefore, the mass ratio of Re and Ir (Re/Ir) on the outer surface of the catalysts was different. Thin shells would be accompanied by a low value of Re/Ir, and the Re/Ir ratio of the RI20 catalyst with the thinnest shell was 0.75. The catalytic activities of catalysts with a Re/Ir ratio of 0.75, which were prepared by the same method as the RI sample, are listed in Table 3. Reducing the value of Re/Ir from 1 to 0.75 will decrease the conversion of glycerol. These results are in agreement with Tomishige's work[16]. Therefore, the high activity of the RI20 catalyst was not due to the decrease in Re/Ir.

Table 4 The average particle size of Ir species calculated from XRD results

catalyst	The average particle size of Ir species (×10^{-6} mm)				Dispersion of reduced catalysts[a]
	Before reaction	After reduction	After reaction for 150h	After reaction for 500h	
RI	6.18	2.24	3.12	3.25	49.2
RI20	4.53	2.11	3.06	3.20	52.2
RI25	5.34	2.13		-	51.9
RI30	5.84	2.19		-	50.3

[a] calculated with the Ir particles obtained from XRD

The XRD analysis was also performed on fresh catalysts (Figure 2a). The diffraction peak at 2θ=21.4° was attributed to amorphous silica gel. Several peaks were observed in the patterns of the fresh catalysts at approximately 26.7°, 34.2° and 53.1°, indexed to IrO_2(110), IrO_2(101) and IrO_2(211) (PDF 01-088-0288). XRD patterns of the samples reduced at 463 K contain new reflections at 2θ=40.5° that are characteristic of metallic iridium (PDF 01-087-0715) (Figure 2b). For the catalysts reacted for 150 h or 500 h, a diffusive diffraction peak of metallic iridium was also observed (Figure 2c). Whether the catalysts were used/not used or reduced/not reduced, all showed no evidence of Re species due to its small particle size. Table 4 shows the average particle size of

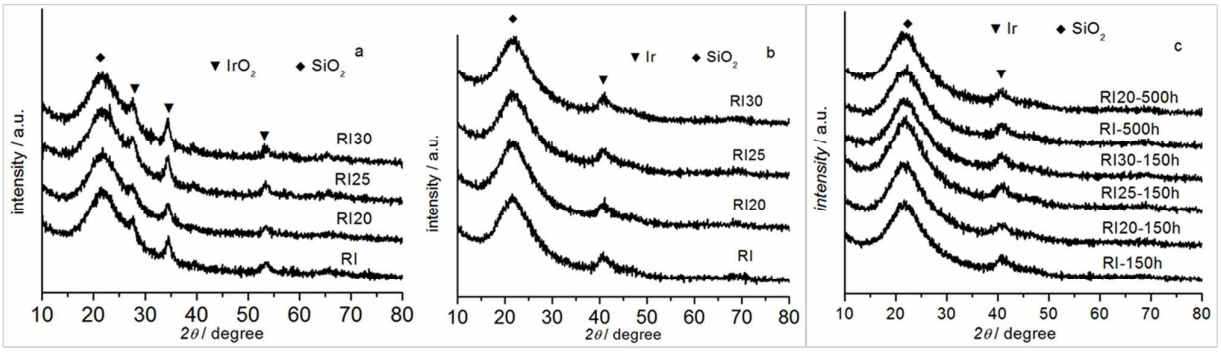

Figure 2 XRD patterns of the RI, RI20, RI25 and RI30 catalysts. (a) before reaction, (b) after reduction at 463K, (c) after reaction.

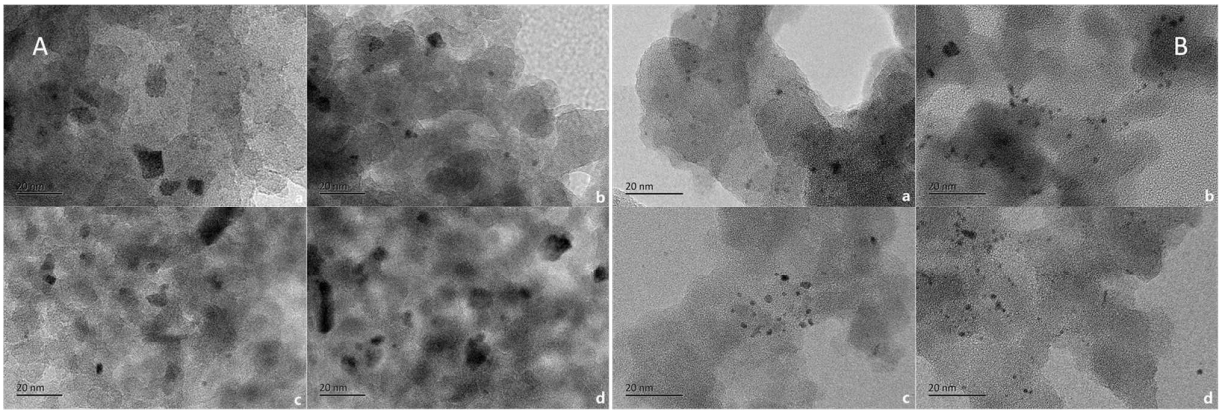

Figure 3 TEM images of catalysts. (A) before reduction, (B) after reduction. (a) RI, (b) RI20, (c) RI25 and (d) RI30..

iridium species of the catalysts that were fresh, reduced and reacted for 150 or 500 h. The average IrO_2 particle sizes of the fresh RI, RI20, RI25 and RI30 catalysts were 6.184×10^{-6}, 4.534×10^{-6}, 5.344×10^{-6} and 5.84×10^{-6} mm, respectively. After reduction, the average Ir particle size of the RI catalyst was 2.24×10^{-6} mm, which was also larger than the particle size of other samples. As the reaction proceeded, the average particle size of Ir increased. The average Ir particle size of the RI catalyst increased from 2.24×10^{-6} mm to 3.12×10^{-6} mm after reaction for 150 h and to 3.25×10^{-6} mm after 500 h, and that of the RI20 catalyst grew from 2.11×10^{-6} mm to 3.06×10^{-6} mm and then to 3.20×10^{-6} mm, respectively. Therefore, the Ir species were the same, and the average particle size of Ir was similar for all of these catalysts.

Figures 3A and 3B show the TEM images of the fresh and reduced catalysts, and the corresponding average Ir particle size statistically calculated from TEM are shown in Table 5. The average IrO_2 particle size on the fresh egg-shell catalysts and the average particle size of Ir species on reduced egg-shell catalysts exhibited smaller mean particle diameters than those of the uniform catalyst, which is consistent with the XRD results. According to the results reported in the literature[30-33], superficial silyl or alkoxyl groups hinder the aggregation of the active metal precursors during drying and reducing processes. The egg-shell catalyst supports were treated in trimethylchlorosilane, causing the trimethylchlorosilane to chemically bond to the surface of the support. The existence of these groups might be the reason that particle sizes on the egg-shell catalysts were smaller than on the uniform catalyst. However, similar dimensions were observed for the reduced catalysts due to the re-dispersion of active components during reduction.

Table 5 The average particle size of Ir species calculated from TEM

catalyst	The average particle size of Ir species ($\times10^{-6}$ mm)	
	Fresh catalysts	Reduced catalysts
RI	6.08	2.14
RI20	4.65	1.85
RI25	5.01	1.88
RI30	5.08	1.89

The TPR profiles of the RI, RI20, RI25, RI30 and mono-component catalysts are shown in Figure 4. The TPR profile of the Re/SiO_2 catalyst contained a single reduction peak with a maximum at 583 K. The signal, which belonged to the reduction of the iridium component, was observed at 493 K in the TPR profile of Ir/SiO_2. The reduction peaks of all Ir catalysts modified by Re have obvious shifts in their reduction temperatures towards lower values, implying an interaction between the Ir and Re species. Contrary to the uniform catalyst, the iridium oxide species were reduced at a much lower temperature for all egg-shell catalysts. Only one peak was observed on the RI and RI30 catalysts at 472 K and 467 K, respectively. This peak might be assigned to the co-reduction of Ir and Re species. However, the TPR profile of the RI20 and RI25 samples contained two reduction peaks. The first peak at 426 K likely resulted from the reduction of small Ir oxide species deposited on the support surface, whereas the second peak at 459 K may have been due to the co-reduction of Ir and Re oxide species.[34-36] The existence of smaller IrO_2, which was revealed by H_2-TPR, is coincident with the results of XRD and TEM.

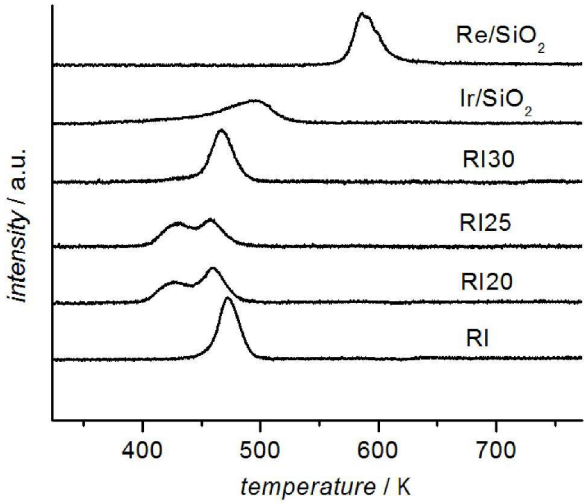

Figure 4 Temperature programmed reduction (TPR) profiles of catalysts.

Information on the metal state was obtained from XPS analysis. Figures S1a and S1b show the Ir 4f XPS spectra of the catalysts before and after reaction for 150 h. For all these fresh catalysts, the binding energy of Ir $4f_{7/2}$ at 61.3-61.7 eV was assigned to Ir^{4+}.[37] After reaction, the XPS spectra showed a peak at approximately 60.7 eV, corresponding to the Ir $4f_{7/2}$ level of Ir^0 species.[38] The valence of Ir species is consistent with the results of XRD. Figures S1c and S1d

present the Re 4f XPS spectra for the fresh catalysts and spent catalysts. The XPS spectra for these catalysts contained a peak at 44.9-45.7 eV. The binding energy of Re $4f_{7/2}$ of Re^{7+} is 46.9 eV.[39, 40] However, the binding energy of Re $4f_{7/2}$ shown in Figure 5 is below 46.9 eV. According to the literature, NH_4ReO_4 is pyrolyzed wholly into Re_2O_7 in air; therefore, the Re species here should be +7.[41] The lower binding energies observed for Re $4f_{7/2}$ compared with that of Re^{7+} species may have been caused by Re species interacting with the support or Ir species. [39] For the catalysts after reaction, the binding energies of Re $4f_{7/2}$ were similar to those for the fresh catalysts, which might have been caused by the oxidation of ReO_x when the spent catalysts were exposed to air.[41]

H_2 chemisorption was carried out to determine the number of iridium active sites, and the results are shown in Table 6. The uptake of hydrogen on all the egg-shell catalysts was greater than that of the uniform catalyst. The H_2 uptake of the RI20 sample which was 1.303 μmol·g^{-1} was the highest among these catalysts. The dispersion of Ir shown in Tables 6 and 4 was calculated from the H_2-chemisorption and XRD results, respectively. The dispersion calculated by the former analysis was much lower than by the latter, implying that only approximately 4% of Ir atoms were exposed on the surface and the other Ir atoms on the surface of the Ir particles might have been covered with Re species. The results obtained from H_2-chemisorption demonstrate that more superficial Ir atoms were present on the egg-shell catalysts than on the uniform catalyst. The uptake of the RI20 catalyst was almost 7 times greater than that of the RI sample. The uptake of the RI25 and RI30 samples were also lager than that of the RI sample. This suggests that the Ir particle size might be smaller on the egg-shell catalysts than on the uniform catalyst, and this result is consistent with the TEM and XRD results.

Table 6 The H_2 uptake and dispersion

Catalyst	H_2 uptake (μmol/g)	Dispersion (%)
		H_2 chemisorption
RI	0.19	0.4
RI20	1.303	2.5
RI25	0.884	1.7
RI30	0.774	1.5
RI20-s60-80	0.499	1.0

Figure 5 shows the NH_3-TPD profiles of fresh catalysts. For TMCS-SiO_2, no NH_3 desorption could be detected in the NH_3-TPD experiment. This indicates that TMCS-SiO_2 had no acidity. A very weak NH_3 desorption peak at a wide temperature range near 573 K was detected over the Ir/SiO_2 catalyst. However, the Re/SiO_2 sample showed one desorption peak at 490 K, and all the catalysts containing Re showed a NH_3 desorption peak at nearly 490 K, suggesting that the Re species constituted the main source of acidity. The supply of acidic sites by Re species was also investigated in the work of He *et al.*[13] Table 7 shows the acidity of all the samples calculated by integrating the NH_3 desorption curves. All the egg-shell catalysts had more acidity than the uniform catalyst, and their acidity might be proportional to the amount of superficial Re species. Therefore, Re species might be better dispersed on the egg-shell catalysts than on the RI sample. Figure 6 shows the NH_3-TPD profiles of RI and RI20 after reacting for 150 h and 500 h. The existence of two desorption peaks suggests that there are two types of acidity on these catalysts. The acidity might be ascribed to Re-OH, and the weak acidity might be assigned to Re-O-Re[42]. The desorption amounts of NH_3 was reduced by about 4.5% when reacted from 150h to 500h.

Table 7 Uptake of NH3 of catalysts

Catalyst	Acidity (μmol·g^{-1})
RI	312.1
RI20	368.9
RI25	363.3
RI30	373.2
Re/SiO_2	239.6

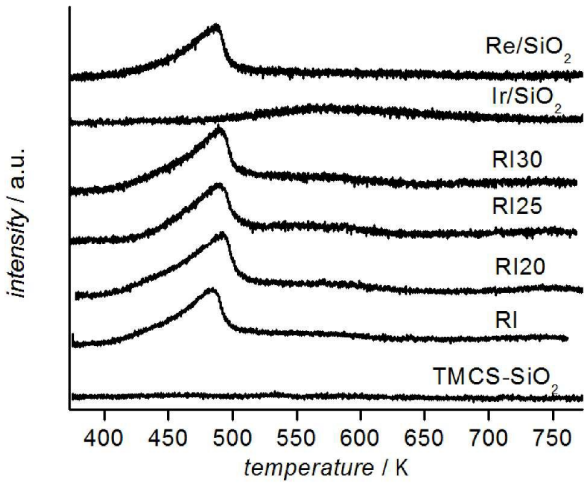

Figure 5 NH_3-TPD profiles of the RI, RI20, RI25, RI30, TMCS-SiO_2, Ir/SiO_2 and Re/SiO_2 catalysts.

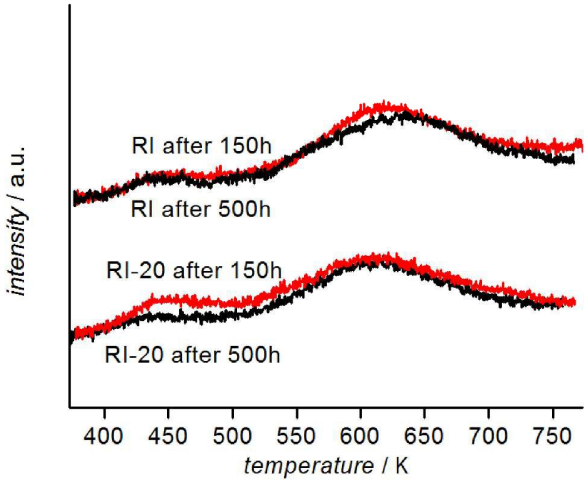

Figure 6 NH_3-TPD profiles of the RI, RI20 catalysts reacting after 150h and 500h.

The results of H_2-chemisorption and NH_3-TPD characterizations showed that the Ir sites in RI20 catalyst were 7-times higher than in RI catalyst, and ReO_x sites in RI20 catalyst were 18% higher than

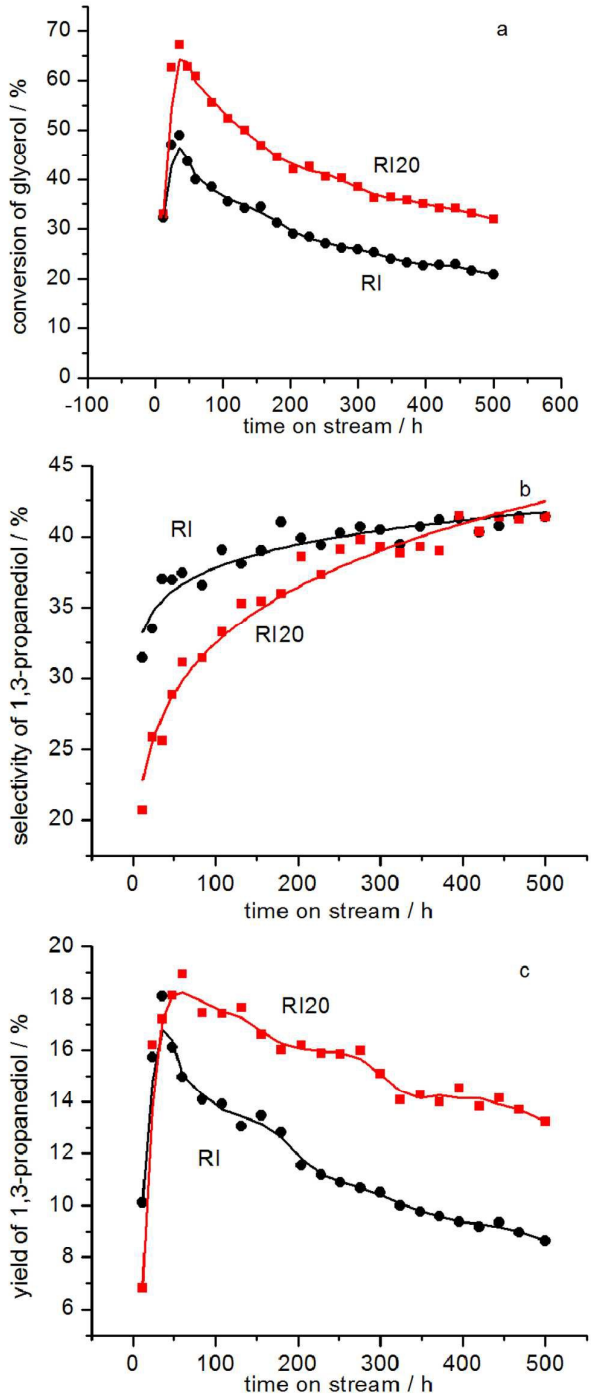

Figure 7 Catalytic performances of RI and RI20 catalysts vs. time on-stream

those in RI catalyst. It could be found in Table 1 that the conversion of glycerol over RI20 catalyst was 24.5% higher than that over RI catalyst. The activity was not proportion to Ir sites or ReO_x sites, which resulted from the fact that the active sites were the interface of Ir and ReO_x, not separate Ir or ReO_x sites[43]. Nonetheless, more Ir and ReO_x sites support more opportunities for the interaction of Ir and ReO_x, which might result in more active sites formation. Therefore, we think that the activity of the catalyst supplying more Ir and ReO_x sites might be higher than others, and it was corresponded to this that the glycerol conversion over RI20-s60-80 catalysts was a little higher than the RI-s60-80 catalyst. However, only a little difference existed between the glycerol conversion over RI20-s60-80 catalyst and over RI-s60-80 catalyst. Therefore, the main reason for higher conversion over RI20 was shorter diffusion distance which could reduce the effect of internal transfer limitation.

500h catalytic performances measurements of catalysts

Figure 7 shows the plot of catalytic performances of RI and RI20 catalysts vs. time on-stream. The conversion of the RI and RI20 catalysts increased to a maximum after 36 h on-stream and then decreased gradually. The selectivities of the RI and RI20 catalysts increased with time on-stream, and the selectivity of the RI20 catalyst increased more quickly. Therefore, the yield of the RI catalyst declined more after the induction period. After reaction for 500 h, the 1,3-propanediol yield of the RI catalyst declined to 48% of its maximum value, whereas that of the RI20 catalyst only declined to 70%. In addition, it took 348 h for the glycerol conversion of the RI catalyst to reduce by half, but 468 h for the RI20 catalyst. Therefore, to some extent, the RI20 catalyst was more stable than the RI catalyst. According to the XRD (Table 4) and NH_3-TPD (Figure 6) results, the Ir particles grew larger and the acidity of RI and RI20 decreased as the reaction progressed, which may have caused the interfacial sites of Ir and ReO_x to decrease. However, the active sites were the interface of Ir and ReO_x. Therefore, fewer interfacial sites of Ir and ReO_x support fewer active sites, which may have caused the deactivation.

Conclusions

Egg-shell Ir-ReO_x catalysts were prepared with silanized support using entrapped air to prevent the impregnation solution from entering into the support pellets. The ethanol concentration of the impregnation solution controlled the thickness of the shells. When a 20% ethanol impregnation solution was used, the best glycerol conversion and 1,3-propanediol yield were obtained. The decreasing diffusion distance in the egg-shell catalyst structure was the primary cause of its high conversion of glycerol. Better heat diffusion hindered the hydrogenolysis of glycerol to 1,2-propanediol, resulting in a higher ratio of 1,3-propandiol to 1,2-propanediol. The generation of smaller particles of IrO_2 on the fresh egg-shell catalysts resulted from the superficial trimethylchlorosilane groups hindering the aggregation of the active metal precursors, but the average particle size of Ir trend to accord after reduction. Catalysts with high conversion lead to greater consecutive hydrogenolysis of 1,3-propanediol. Therefore, there was higher conversion along with lower 1,3-propandiol selectivity when using the egg-shell catalysts. However, the yields of removal secondary hydroxyl groups ($Y_{2\text{-}OH}$) on the egg-shell catalysts were higher than on the uniform catalyst. Our results also suggest that the RI20 catalyst was more stable than the RI catalyst. The egg-shell catalysts could promote the conversion of glycerol while maintaining an acceptable pressure

gradient which is important in industrial fixed-bed reactors. Therefore, our study provides a basis for practical industrial applications.

Notes and references

1. C. Cardona, J. Posada and M. Montoya, *Proc. Eur. Congr. Chem. Eng.*, 2007, 16-20.
2. J. Regalbuto, *Comput. Chem. Eng.*, 2010, **34**, 1393-1396.
3. P. Gallezot, *Chem. Soc. Rev.*, 2012, **41**, 1538-1558.
4. G. Knothe, S. C. Cermak and R. L. Evangelista, *Fuel*, 2012, **96**, 535-540.
5. M. McCoy, *Chemical & Engineering News*, 2006, **84**, 7-7.
6. J. Gong and F. You, *ACS Sustainable Chemistry & Engineering*, 2015, **3**, 82-96.
7. A. Behr, J. Eilting, K. Irawadi, J. Leschinski and F. Lindner, *Green Chem.*, 2008, **10**, 13-30.
8. Y. Nakagawa and K. Tomishige, *Catal. Sci. Technol*, 2011, **1**, 179.
9. O. M. Daniel, A. DeLaRiva, E. L. Kunkes, A. K. Datye, J. A. Dumesic and R. J. Davis, *ChemCatChem*, 2010, **2**, 1107-1114.
10. Y. Shinmi, S. Koso, T. Kubota, Y. Nakagawa and K. Tomishige, *Appl. Catal. B: Environ*, 2010, **94**, 318-326.
11. Y. Nakagawa, Y. Shinmi, S. Koso and K. Tomishige, *J. Catal.*, 2010, **272**, 191-194.
12. L. Ma and D. He, *Top. Catal.*, 2009, **52**, 834-844.
13. Y. Li, H. Liu, L. Ma and D. He, *RSC. Adv.*, 2014, **4**, 5503.
14. Y. Nakagawa, X. Ning, Y. Amada and K. Tomishige, *Appl. Catal. A: Gen*, 2012, **433-434**, 128-134.
15. Y. Nakagawa, K. Mori, K. Chen, Y. Amada, M. Tamura and K. Tomishige, *Appl. Catal. A: Gen*, 2013, **468**, 418-425.
16. Y. Amada, Y. Shinmi, S. Koso, T. Kubota, Y. Nakagawa and K. Tomishige, *Appl. Catal. B: Environ*, 2011, **105**, 117-127.
17. K. Tomishige, Y. Nakagawa and M. Tamura, 2014, **353**, 127-162.
18. N. Carrara, J. M. Badano, C. Betti, C. Lederhos, I. Rintoul, F. Coloma-Pascual, C. Vera and M. Quiroga, *Catal. Commun.*, 2015, **61**, 72-77.
19. A. Drelinkiewicza, A. Waksmundzka, W. Makowski, J. W. Sobczak, A. Krol and A. Zieba, *Catal. Lett.*, 2004, **94**, 143-156.
20. J. M. Badano, C. Betti, I. Rintoul, J. Vich-Berlanga, E. Cagnola, G. Torres, C. Vera, J. Yori and M. Quiroga, *Appl. Catal. A: Gen*, 2010, **390**, 166-174.
21. T. B. Lin and T. C. Chou, *Ind. Eng. Chem. Res.*, 1995, **34**, 128-134.
22. J. Li, Y. Ding, X. Li, G. Jiao, T. Wang, W. Chen and H. Luo, *Chem. Commun.*, 2008, DOI: 10.1039/b813641f, 5954.
23. S. A. Gardezi, L. Landrigan, B. Joseph and J. T. Wolan, *Ind. Eng. Chem. Res.*, 2012, **51**, 1703-1712.
24. Y. Qiu, J. Chen and J. Zhang, *Catal. Commun.*, 2007, **8**, 508-512.
25. B. Liu, Y. M. Chai, Y. K. Liu, Y. J. Wang, Y. Q. Liu and C. G. Liu, *Fuel*, 2012, **95**, 457-463.
26. T. A. Nijhuis, F. M. Dautzenberg and J. A. Moulijn, *Chem. Eng. Sci.*, 2003, **58**, 1113-1124.
27. K. Ouyang, Y. Huang, H. Chen, T. Li, F. Cao and D. Fang, *Frontiers of Chemical Science and Engineering*, 2010, **5**, 67-73.
28. C. Deng, L. Leng, X. Duan, J. Zhou, X. Zhou and W. Yuan, *J. Mol. Catal. A: Chem.*, 2015, **410**, 81-88.
29. C. Deng, X. Duan, J. Zhou, X. Zhou, W. Yuan and S. L. Scott, *Catal. Sci. Technol.*, 2015, **5**, 1540-1547.
30. D. Jiang, Y. Ding, Z. Pan, W. Chen and H. Luo, *Catal. Lett.*, 2007, **121**, 241-246.
31. Y. Zhang, K. Hanayama and N. Tsubaki, *Catal. Commun.*, 2006, **7**, 251-254.
32. J. Cortes, R. Jimenez and P. Araya, *Catal. Lett.*, 2002, **82**, 255-259.
33. L. Jia, L. Jia, D. Li, B. Hou, J. Wang and Y. Sun, *Natural Gas Chemical Industry*, 2010, **35**, 6-11.
34. B. Li, X. Qian and X. Wang, *International Journal of Hydrogen Energy*, 2015, **40**, 8081-8092.
35. L. Shi, D. Li, B. Hou, Y. Wang and Y. Sun, *Fuel Process. Technol.*, 2010, **91**, 394-398.
36. K. Baranowska and J. Okal, *Appl. Catal. A: Gen*, 2015, **499**, 158-167.
37. J. Riga, C. Tenretnoel, J. J. Pireaux, R. Caudano, J. J. Verbist and Y. Gobillon, *Phys. Scr.*, 1977, **16**, 351-354.
38. C. Campos, C. Torres, M. Oportus, M. A. Peña, J. L. G. Fierro and P. Reyes, *Catal. Today*, 2013, **213**, 93-100.
39. T. Tsoncheva, S. Vankova, O. Bozhkov and D. Mehandjiev, *Can. J. Chem.*, 2007, **85**, 118-123.
40. Youzhu Yuan and Y. Iwasawa, *J. Phys. Chem. B*, 2002, **106**, 4441-4449.
41. M. Bai, Z.-h. Liu, L.-j. Zhou, Z.-y. Liu and C.-f. Zhang, *Trans. Nonferrous Met. Soc. China*, 2013, **23**, 538-542.
42. A. Ciftci, B. Peng, A. Jentys, J. A. Lercher and E. J. M. Hensen, Appl. Catal. A: Gen, 2012, 431-432, 113-119.
43. Y. Amada, H. Watanabe, M. Tamura, Y. Nakagawa, K. Okumura and K. Tomishige, J. Phys. Chem. C, 2012, 116, 23503-23514.

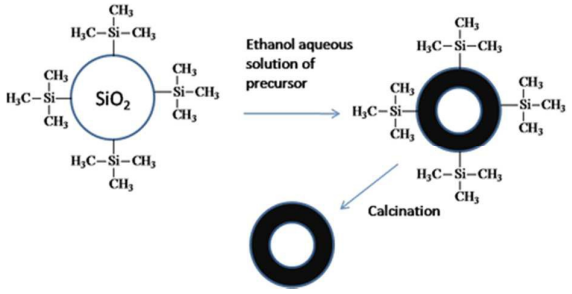

The egg-shell catalysts could promote the conversion of glycerol while maintaining an acceptable pressure gradient.